Editors' Suggestion | Featured in Physics

Observation of Topological Magnon Insulator States in a Superconducting Circuit

W. Cai,[1,*] J. Han,[1,*] Feng Mei,[2,3,†] Y. Xu,[1] Y. Ma,[1] X. Li,[1] H. Wang,[1] Y. P. Song,[1]
Zheng-Yuan Xue,[4] Zhang-qi Yin,[1] Suotang Jia,[2,3] and Luyan Sun[1,‡]

[1]*Center for Quantum Information, Institute for Interdisciplinary Information Sciences, Tsinghua University, Beijing 100084, China*

[2]*State Key Laboratory of Quantum Optics and Quantum Optics Devices, Institute of Laser Spectroscopy, Shanxi University, Taiyuan, Shanxi 030006, China*

[3]*Collaborative Innovation Center of Extreme Optics, Shanxi University, Taiyuan, Shanxi 030006, China*

[4]*Guangdong Provincial Key Laboratory of Quantum Engineering and Quantum Materials, and School of Physics and Telecommunication Engineering, South China Normal University, Guangzhou 510006, China*

(Received 8 April 2019; published 20 August 2019)

Searching topological states in artificial systems has recently become a rapidly growing field of research. Meanwhile, significant experimental progress on observing topological phenomena has been made in superconducting circuits. However, topological insulator states have not yet been reported in this system. Here, for the first time, we experimentally realize a tunable dimerized spin chain model and observe the topological magnon insulator states in a superconducting qubit chain. Via parametric modulations of the qubit frequencies, we show that the qubit chain can be flexibly tuned into topologically trivial or nontrivial magnon insulator states. Based on monitoring the quantum dynamics of a single-qubit excitation in the chain, we not only measure the topological winding numbers, but also observe the topological magnon edge and defect states. Our experiment exhibits the great potential of tunable superconducting qubit chain as a versatile platform for exploring noninteracting and interacting symmetry-protected topological states.

DOI: 10.1103/PhysRevLett.123.080501

Topological insulators are new states of matter beyond Landau symmetry breaking theory, signified by topological invariants and topological edge states, and now lie at the forefront of condensed matter physics [1,2]. The concept of topological insulators recently has been intensively studied and has also been expanded to artificial systems, including ultracold atomic [3–5], photonic [6,7], and mechanical [8,9] systems. Nevertheless, as a result of the difficulties in extracting the Berry curvature in photonic and mechanical systems and in engineering edges in optical lattices, it is still challenging to experimentally observe both the topological invariants and the topological edge states in a separate artificial topological system.

Superconducting circuits now have become one of the leading quantum platforms for implementing scalable quantum computation [10–12] and large-scale quantum simulation [13–15]. In particular, topological effects recently have also been experimentally studied in superconducting circuits. Specifically, topological concepts have been investigated in the parameter space of superconducting qubits [16–19] and the phase space of superconducting resonators [20,21], synthetic gauge fields [22–25] and the Hofstadter butterfly [26] have been realized in a superconducting qubit chain, and topological phenomena have also been observed in a network of superconducting flux qubits [27]. However, due to the challenges in engineering a topological chain with tunable qubit couplings and the lack of methods in detecting the topology of the qubit chain system, topological insulator states still have not been experimentally observed before in the superconducting system.

In this Letter, we experimentally demonstrate the first observation of topological insulator states in a tunable superconducting transmon qubit chain, which exhibits both the nontrivial topological invariants and topological edge states. Our experiment is based on realizing a dimerized spin chain model, which supports topologically trivial or nontrivial magnon insulator states dependent on the qubit coupling configurations. We demonstrate that such configurations can be flexibly tuned via parametrical modulations of the qubit frequencies *in situ* [28–32]. Through exciting one of the qubits in the chain and then monitoring its quantum dynamics, we further show that the topological winding numbers can be directly measured. By tuning the qubit chain with odd and even number of qubits, the localization and hybridization of topological edge states are observed, respectively. Via locally tuning the qubit couplings, we also exhibit that a topological defect can be easily created and probed.

Distinct from previous systems studying the topological states of noninteracting bosons in a lattice [3–9], the superconducting system allows the study of the topological states of magnons (qubit excitations) in an interacting spin

(qubit) chain, where magnons are bosonic quasiparticle excitations around the ground state of the spin chain [33,34] and are interacting hard-core bosons. Although our experiment investigates the single-excitation case and observes the resulted noninteracting symmetry-protected topological magnon insulator states, it paves the way for further study of bosonic interacting symmetry-protected topological states [35,36] when introducing multiple excitations into a longer qubit chain. Realizing interacting symmetry-protected topological states currently is still a great challenge [37] and cannot be achieved in previously reported noninteracting topological systems [3–9]. Our experiment represents the first step towards realizing such states with a qubit chain system.

The experimental model is based on a dimerized spin chain, which describes a one-dimensional spin lattice with two spins per unit cell and different intra- and intercell hopping amplitudes, as shown in Fig. 1(a). We implement such a model in a superconducting qubit chain [38], where each unit cell contains two qubits labeled by a and b. The resulting qubit chain can be described by the dimerized spin chain Hamiltonian after the rotating wave approximation

$$\hat{H} = \sum_{x=1}^{N} (J_1 \hat{\sigma}_{a_x}^{+} \hat{\sigma}_{b_x}^{-} + J_2 \hat{\sigma}_{b_x}^{+} \hat{\sigma}_{a_{x+1}}^{-} + \text{H.c.}), \tag{1}$$

where x is the unit cell index, N is the number of the unit cells, J_1 and J_2 are the intra- and intercell qubit couplings, respectively, and $\sigma_{a_x}^{+}$ ($\sigma_{a_x}^{-}$) is the raising (lowering) operator associated with qubit a_x. The single-qubit excitation in this spin chain is called a magnon in condensed matter physics [33,34]. In the single-qubit excitation case, its topology is the same as that of the Su-Schrieffer-Heeger model [39–42], which has two distinct topological insulator states characterized by topological winding numbers. However, the difference from the Su-Schrieffer-Heeger model is that the system studied in our experiment is an interacting spin chain and can be further used to realize interacting symmetry-protected topological states. Moreover, magnons are bosonic quasiparticle excitations around the ground state of the spin chain; therefore, the topological states observed here are associated with excited states instead of ground states. When the qubit couplings are tuned into $J_1 < J_2$ ($J_1 > J_2$), the topological winding number $\nu = 1$ ($\nu = 0$) and the system supports a topologically nontrivial (trivial) magnon insulator state (see Supplemental Material [43]).

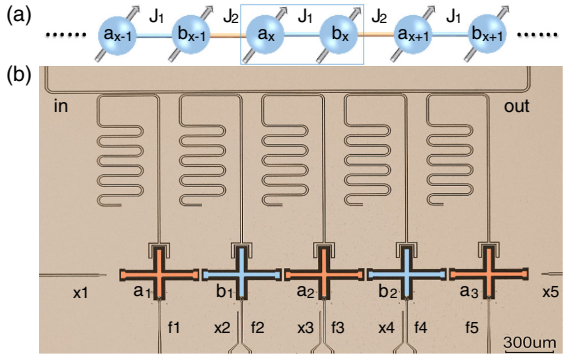

FIG. 1. A dimerized qubit chain. (a) The schematic setup of a qubit chain, where x denotes the unit cell index. Each unit cell has two qubits a and b. The intra- and interunit cell couplings are J_1 and J_2, respectively. (b) Five cross-shaped transmon qubits (X mons, a_1, b_1, a_2, b_2, and a_3) arranged in a linear array. Each qubit is coupled to a separate $\lambda/4$ resonator for simultaneous and individual readout and has independent XY and Z controls (labeled as "x" and "f", respectively).

We implement the experiment in a superconducting circuit [10,11,51] consisting of five cross-shaped transmon qubits (X mons, a_1, b_1, a_2, b_2, and a_3) [44,45] arranged in a linear array with fixed capacitive nearest-neighbor couplings, as shown in Fig. 1(b). Each qubit has independent XY and Z controls. Separate $\lambda/4$ resonators with different frequencies couple to individual qubits for independent readouts. The average qubit $T_1 \approx 18$ μs and $T_2^* \approx 17$ μs at the frequency sweet spots. We use a Josephson parametric amplifier [46,47], a gain over 20 dB, and a bandwidth of about 260 MHz for high-fidelity single-shot measurements of the qubits. To overcome the readout imperfections, in addition, we use a calibration matrix to reconstruct the readout results based on Bayes' rule.

The topologically trivial and nontrivial phases require different qubit-qubit coupling configurations, necessitating full control of the effective couplings between neighboring qubits. Tunable couplings through parametrical modulations of the qubit frequencies can be realized *in situ* without increasing circuit complexity [28–32], and therefore are ideal for topological simulations. We adopt this technique throughout our experiment to realize the required neighboring qubit coupling strengths as described in Eq. (1).

Explicitly, we apply

$$\omega_{id} = \omega_{o\_id} + \varepsilon_{id} \sin(\mu_{id} t + \varphi_{id}), \tag{2}$$

where ω_{o_id} is the mean operating frequency, ε_{id}, μ_{id}, and φ_{id} are the modulation amplitude, frequency, and phase, respectively, for the qubit $id = a_x, b_x$ in the chain. By neglecting the higher order oscillating terms and under the resonant conditions $\omega_{o\_b_x} - \omega_{o\_a_x} = \mu_{b_x}$ or $\omega_{o\_b_{x-1}} - \omega_{o\_a_x} = \mu_{a_x}$, the effective coupling strengths are

$$\begin{aligned} J_1 &= g_{a_x,b_x} \mathcal{J}_1(\alpha_{b_x}) \mathcal{J}_0(\alpha_{a_x}) e^{i(\varphi_{b_x} + \pi/2)}, \\ J_2 &= g_{b_{x-1},a_x} \mathcal{J}_1(\alpha_{a_x}) \mathcal{J}_0(\alpha_{b_{x-1}}) e^{-i(\varphi_{a_x} - \pi/2)}, \end{aligned} \tag{3}$$

where $\mathcal{J}_m(\alpha)$ is the mth Bessel function of the first kind and g_{a_x,b_x} is the static capacitive coupling strength between neighboring qubits. Both J_1 and J_2 can be conveniently tuned via changing $\alpha_{id} = \varepsilon_{id}/\mu_{id}$ of the external modulation. Note that the qubit at the edge (for example, a_1) could be stationary without parametric modulation, while the

middle qubit can be parametrically modulated with two independent sinusoidal drives in order to tune the coupling strengths with its two neighboring qubits, respectively. The experimental setup, device parameters, and parametric modulation parameters are all presented in detail in the Supplemental Material [43].

We first demonstrate that the topological winding number can be measured by single-magnon quantum dynamics in a chain of four transmon qubits, provided the qubit chain is initially prepared in a single-magnon bulk state. This dynamic method for measuring the topological winding number was originally proposed in a linear-optics system for studying discrete-time quantum walk [48]. We choose to excite one of the middle qubits to the excited state $|e\rangle$ and leave the other qubits in the ground state $|g\rangle$, leading to an initial state of the system $|\psi(t=0)\rangle = |gegg\rangle$. After an evolution time t, the state of the system becomes $|\psi(t)\rangle = e^{-i\hat{H}t}|\psi(t=0)\rangle$. To reveal the relationship between this dynamics and the topological winding number, we introduce the chiral displacement (CD) operator $\hat{P}_d = \sum_{x=1}^{2} x(\hat{P}^e_{a_x} - \hat{P}^e_{b_x})$ with $\hat{P}^e_{id} = |e\rangle_{id}\langle e|$ $(id = a_x, b_x)$. In the long-time limit, the topological winding number ν can be extracted from the time-averaged CD, $\nu = \lim_{T\to\infty}(2/T)\int_0^T dt\bar{P}_d(t)$, where T is the evolution time and $\bar{P}_d(t) = \langle\psi(t)|\hat{P}_d|\psi(t)\rangle$ is the CD associated with the dynamics of the single-magnon state (see Supplemental Material [43]). As we can see, the topological winding number is two times the time-averaged CD, i.e., the oscillation center of the CD versus time. Experimentally, to measure the time-averaged CD we only need to track the time evolution of the excitation for each qubit.

In the experiment, as shown in Figs. 2(a) and 2(b), we tune the qubit chain into two configurations with the qubit coupling dimerization $J_1 > J_2$ and $J_1 < J_2$, corresponding to the topologically trivial and nontrivial magnon insulator states, respectively. After preparing the initial state $|\psi(0)\rangle$, we measure the time evolution (with an interval of 1 ns) of the qubit excitation of the four qubits and show the experimental data in Figs. 2(c) and 2(d). The measured excitation evolutions agree well with the theoretical predictions. Based on these time-resolved excitation data for each qubit, we directly derive the time evolution of CDs and plot them in Figs. 2(e) and 2(f). Clearly the two curves oscillate around two different center values, qualitatively giving the signature of different topological winding numbers. The evolution time in our experiment is chosen as 1 μs, during which the experimentally measured time-averaged CDs are 0.015 and 0.359 for the topologically trivial and nontrivial cases, respectively. Both experiments agree very well with the theoretically expected values of 0 and 0.378, giving the experimentally measured topological winding numbers $v = 0.030$ and $\nu = 0.718$ for the two cases. The measured winding number for the topologically trivial case is quite close to the ideal value.

The reasons for the difference in the topologically nontrivial case between the measured winding number $\nu = 0.718$ and the ideal value $\nu = 1$ are that both the evolution time and the qubit chain we choose are not long enough and there is also inevitable system decoherence. Nevertheless, our experimental data within 1 μs agree excellently with the theoretical expectation and demonstrate the validness of the method using single-magnon dynamics to measure the topological winding number. The clear distinction between the measured nontrivial and trivial topological winding numbers thus can unambiguously distinguish the topologically nontrivial and trivial magnon insulator states.

The second hallmark for topological magnon insulator states is the existence of topological magnon edge states at the boundary. When the qubit chain is tuned into the topological magnon insulator state, according to bulk-edge correspondence [1,2], the topological magnon edge state will emerge at

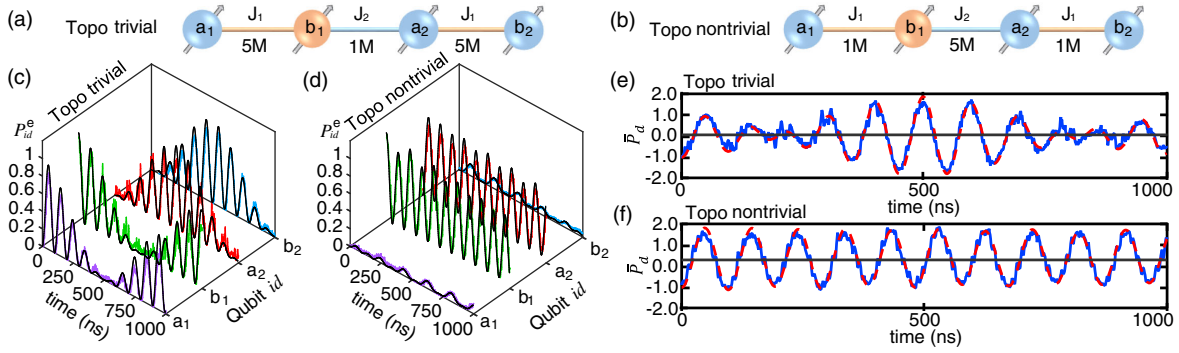

FIG. 2. Topological winding number measurements. (a),(b) Schematic of the experiments in which only a_1, b_1, a_2, and b_2 are used without a_3. The couplings between neighboring qubits are configured into J_1-J_2-J_1 = 5-1-5 (MHz) [(a) topologically trivial] and J_1-J_2-J_1 = 1-5-1 (MHz) [(b) topologically nontrivial], respectively. (c),(d) Time evolution of the qubit excitation P^e_{id} for $id = a_1, b_1, a_2, b_2$ for the two different coupling configurations. Dots are experimental data, while solid lines are calculated from the ideal Hamiltonian [Eq. (1)] with the measured system decoherence for an initial state $|gegg\rangle$. (e),(f) Time evolution of $\bar{P}_d = (P^e_{a_1} - P^e_{b_1}) + 2(P^e_{a_2} - P^e_{b_2})$ for the two cases. Dots are experimental data (averaged 5000 times), red dashed lines are from numerical simulations, and the black horizontal lines represent the oscillation centers.

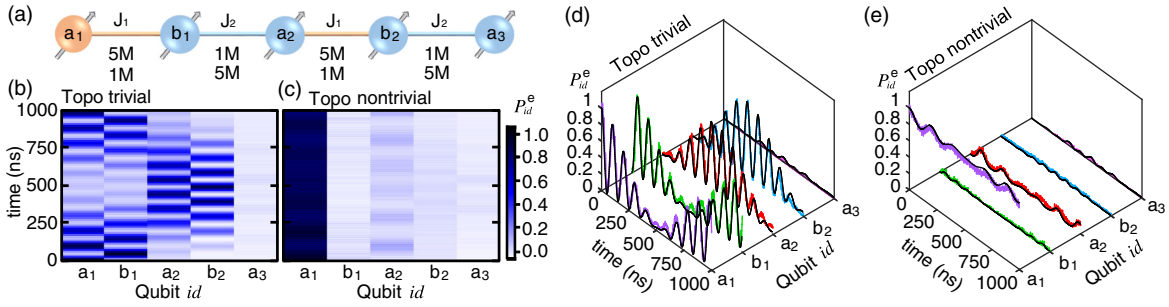

FIG. 3. Observation of topological magnon edge states. (a) Schematic of the experiment in which all five qubits have been used. The couplings between neighboring qubits are configured into J_1-J_2-J_1-J_2 = 5-1-5-1 (MHz) (topologically trivial) and J_1-J_2-J_1-J_2 = 1-5-1-5 (MHz) (topologically nontrivial), respectively. (b),(c) Two-dimensional representation of time evolutions of all qubits' excited state populations $[P^e_{id}(t)]$. (d),(e) Time evolution of P^e_{id}. Dots are experimental data, while solid lines are calculated from the ideal Hamiltonian [Eq. (1)] with the measured system decoherence for an initial state $|eggg\rangle$.

the edges of the qubit chain. The wave functions of the left and right magnon edge states can be analytically derived as $|\psi_L\rangle = \sum_x (-1)^x (J_1/J_2)^x \sigma^+_{a_x} |gg\cdots gg\rangle$ and $|\psi_R\rangle = \sum_x (-1)^{N-x} (J_1/J_2)^{N-x} \sigma^+_{b_x} |gg\cdots gg\rangle$, respectively (see Supplemental Material [43]). It turns out that the magnon in the left (right) edge state only occupies the a-type (b-type) qubit and is maximally distributed in the leftmost (rightmost) qubit. Such two features provide a means to observe the topological magnon edge states. However, the coupling between the left and right magnon edge states is very large due to the finite lattice size effect, and we cannot unambiguously observe the left or right magnon edge state localization in a short qubit chain. This problem can be solved by tuning the qubit chain with an odd number of qubits, where the right topological magnon edge state has been artificially removed [43].

Now we show that the left topological magnon edge state can be clearly observed in a chain of five qubits where there is no right topological magnon edge state [43]. As shown in Fig. 3(a), we can tune the qubit couplings in a chain of five qubits to make the system topologically trivial and nontrivial, respectively. Initially, the leftmost a-type qubit is excited and a single magnon has been put on the leftmost qubit with the initial system state $|\psi(t=0)\rangle = |eggg\rangle$. Then, we let this magnon state evolve for a certain time and measure the time evolution of the magnon density in the qubit chain. The results for the qubit chain being tuned into the topologically trivial state are shown in Fig. 3(b). As expected, there is no magnon edge state localization and the wave packet has a ballistic spread vs time, which is a typical feature of a bulk Bloch state. The reason is that the initial magnon state in this case is a superposition of different bulk states; therefore, it evolves in the qubit chain via the bulk state wave packets and does not support edge state localization.

In contrast, if the qubit chain is tuned into the topologically nontrivial state that can support left magnon edge states, as shown in Fig. 3(c), the measured magnon density is always maximal in the leftmost qubit. This is because the initial magnon state $|\psi(t=0)\rangle$ has a large overlap with the left magnon edge state $|\psi_L\rangle$. The magnon state thus mainly evolves in the qubit chain based on the edge state wave packet and always maximally localizes in the leftmost qubit. Moreover, the magnon only populates the a-type qubits, also satisfying the feature of the left topological magnon edge state as mentioned before. These two features prove the existence of the left topological magnon edge state and clearly indicate that the system is topologically nontrivial. In Figs. 3(d) and 3(e), we also find that the measured qubit excitation evolutions agree excellently with the theoretical predictions.

The third important topological aspect is the emergence of a topological defect state at the interface between topologically trivial and nontrivial regions [39]. When the qubit chain is tuned with two different topological configurations, a topological interface separating the topologically trivial ($J_1 > J_2$) and nontrivial ($J_1 < J_2$) regions can be created, where a topological magnon defect state is trapped. As shown in Fig. 4(a), we can create such a defect state at qubit a_2 in a chain of five qubits. The magnon in the

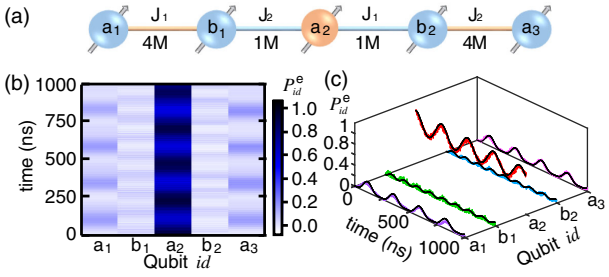

FIG. 4. Observation of topological magnon defect states. (a) Schematic of the experiment. The couplings between neighboring qubits are tuned into J_1-J_2-J_1-J_2 = 4-1-1-4 (MHz). (b) Two-dimensional representation of time evolutions of all qubits' excited state populations. (c) Time evolutions of P^e_{id}. Dots are experimental data, while solid lines are calculated from the ideal Hamiltonian [Eq. (1)] with the measured system decoherence for an initial state $|ggegg\rangle$.

topological defect state should only occupy a-type qubits and its density should be maximally distributed in qubit a_2 (see Supplemental Material [43]). Experimentally, we initially excite qubit a_2 and prepare the system in $|\psi(t=0)\rangle = |ggegg\rangle$. Such an initial state has a large overlap with the wave function of the topological magnon defect state. If the system has the topological defect state, the magnon will propagate in the qubit chain via the defect state wave packet. In the experiment, after evolving $|\psi(t=0)\rangle$ for certain time, we measure the final magnon density distribution in the qubit chain. The experimental results are shown in Fig. 4(b) and indeed indicate that the magnon is maximally localized in the center qubit a_2 and only has populations in the a-type qubits, unambiguously demonstrating the existence of a topological magnon defect state. The time evolutions of qubit excitation for the five qubits are also shown in Fig. 4(c), agreeing well with the theoretical expectations.

In conclusion, our experiment has demonstrated the potential of a tunable superconducting qubit chain as a versatile platform for exploring topology, including measuring topological invariants and observing topological edge and defect states. Since multiple-qubit excitations can be precisely prepared in this system, our study paves the way for further using a longer qubit chain to realize interacting symmetry-protected topological states [35,36] and probe symmetry-protected ground state degeneracy [37]. Through periodically driving the qubit frequencies, nonequilibrium interacting symmetry-protected topological states also can be studied [52]. Additionally, it is also quite interesting to study how the topological states in the qubit chain helps to accomplish topologically protected quantum information processing tasks [53,54]. In addition to superconducting qubits, our experiment can be generalized to other qubit systems and could attract broad interests in exploring symmetry-protected topological states with different quantum computing platforms.

This work is supported by the National Key Research and Development Program of China (2017YFA0304203, 2017YFA0304303, 2016YFA0301803), Natural National Science Foundation of China (11474177, 11604392, 11434007, 11874156, 61771278), Changjiang Scholars and Innovative Research Team in University of Ministry of Education of China (PCSIRT)(IRT_17R70), Fund for Shanxi 1331 Project Key Subjects Construction, and 111 Project (D18001). L. S. also thanks R. Vijay and his group for help on the parametric amplifier measurements.

*These two authors contributed equally to this work.
†meifeng@sxu.edu.cn
‡luyansun@tsinghua.edu.cn

[1] M. Z. Hasan and C. L. Kane, Colloquium: Topological insulators, Rev. Mod. Phys. **82**, 3045 (2010).
[2] X.-L. Qi and S.-C. Zhang, Topological insulators and superconductors, Rev. Mod. Phys. **83**, 1057 (2011).
[3] N. Goldman, J. C. Budich, and P. Zoller, Topological quantum matter with ultracold gases in optical lattices, Nat. Phys. **12**, 639 (2016).
[4] D.-W. Zhang, Y.-Q. Zhu, Y. X. Zhao, H. Yan, and S.-L. Zhu, Topological quantum matter with cold atoms, Adv. Phys. **67**, 253 (2019).
[5] N. R. Cooper, J. Dalibard, and I. B. Spielman, Topological bands for ultracold atoms, Rev. Mod. Phys. **91**, 015005 (2019).
[6] L. Lu, J. D. Joannopoulos, and M. Soljacic, Topological photonics, Nat. Photonics **8**, 821 (2014).
[7] T. Ozawa, H. M. Price, A. Amo, N. Goldman, M. Hafezi, L. Lu, M. C. Rechtsman, D. Schuster, J. Simon, O. Zilberberg, and I. Carusotto, Topological photonics, Rev. Mod. Phys. **91**, 015006 (2019).
[8] S. D. Huber, Topological mechanics, Nat. Phys. **12**, 621 (2016).
[9] G. Ma, M. Xiao, and C. T. Chan, Topological phases in acoustic and mechanical systems, Nat. Rev. Phys. **1**, 281 (2019).
[10] J. Q. You and F. Nori, Atomic physics and quantum optics using superconducting circuits, Nature (London) **474**, 589 (2011).
[11] M. H. Devoret and R. J. Schoelkopf, Superconducting circuits for quantum information: An outlook, Science **339**, 1169 (2013).
[12] C. Neill *et al.*, A blueprint for demonstrating quantum supremacy with superconducting qubits, Science **360**, 195 (2018).
[13] I. Buluta and F. Nori, Quantum simulators, Science **326**, 108 (2009).
[14] A. A. Houck, H. E. Türeci, and J. Koch, On-chip quantum simulation with superconducting circuits, Nat. Phys. **8**, 292 (2012).
[15] I. M. Georgescu, S. Ashhab, and F. Nori, Quantum simulation, Rev. Mod. Phys. **86**, 153 (2014).
[16] M. D. Schroer, M. H. Kolodrubetz, W. F. Kindel, M. Sandberg, J. Gao, M. R. Vissers, D. P. Pappas, A. Polkovnikov, and K. W. Lehnert, Measuring a Topological Transition in an Artificial Spin-1/2 System, Phys. Rev. Lett. **113**, 050402 (2014).
[17] P. Roushan, C. Neill, Y. Chen, M. Kolodrubetz *et al.*, Observation of topological transitions in interacting quantum circuits, Nature (London) **515**, 241 (2014).
[18] T. Wang, Z. Zhang, L. Xiang, Z. Gong, J. Wu, and Y. Yin, Simulating a topological transition in a superconducting phase qubit by fast adiabatic trajectories, Sci. China Phys. Mech. Astron. **61**, 047411 (2018).
[19] X. Tan, D.-W. Zhang, Q. Liu, G. Xue, H.-F. Yu, Y.-Q. Zhu, H. Yan, S.-L. Zhu, and Y. Yu, Topological Maxwell Metal Bands in a Superconducting Qutrit, Phys. Rev. Lett. **120**, 130503 (2018).
[20] V. V. Ramasesh, E. Flurin, M. Rudner, I. Siddiqi, and N. Y. Yao, Direct Probe of Topological Invariants Using Bloch Oscillating Quantum Walks, Phys. Rev. Lett. **118**, 130501 (2017).
[21] E. Flurin, V. V. Ramasesh, S. Hacohen-Gourgy, L. S. Martin, N. Y. Yao, and I. Siddiqi, Observing Topological

Invariants Using Quantum Walks in Superconducting Circuits, Phys. Rev. X **7**, 031023 (2017).
[22] P. Roushan *et al.*, Chiral ground-state currents of interacting photons in a synthetic magnetic field, Nat. Phys. **13**, 146 (2017).
[23] Y.-P. Wang, W. Wang, Z.-Y. Xue, W.-L. Yang, Y. Hu, and Y. Wu, Realizing and characterizing chiral photon flow in a circuit quantum electrodynamics necklace, Sci. Rep. **5**, 8352 (2015).
[24] Y.-P. Wang, W.-L. Yang, Y. Hu, Z.-Y. Xue, and Y. Wu, Detecting topological phases of microwave photons in a circuit quantum electrodynamics lattice, npj Quantum Inf. **2**, 16015 (2016).
[25] C. Owens, A. LaChapelle, B. Saxberg, B. M. Anderson, R. Ma, J. Simon, and D. I. Schuster, Quarter-flux Hofstadter lattice in a qubit-compatible microwave cavity array, Phys. Rev. A **97**, 013818 (2018).
[26] P. Roushan *et al.*, Spectroscopic signatures of localization with interacting photons in superconducting qubits, Science **358**, 1175 (2017).
[27] A. D. King *et al.*, Observation of topological phenomena in a programmable lattice of 1,800 qubits, Nature (London) **560**, 456 (2018).
[28] L. Zhou, S. Yang, Y.-x. Liu, C. P. Sun, and F. Nori, Quantum Zeno switch for single-photon coherent transport, Phys. Rev. A **80**, 062109 (2009).
[29] J. D. Strand, M. Ware, F. Beaudoin, T. A. Ohki, B. R. Johnson, A. Blais, and B. L. T. Plourde, First-order sideband transitions with flux-driven asymmetric transmon qubits, Phys. Rev. B **87**, 220505(R) (2013).
[30] Y. Wu, L. Yang, M. Gong, Y. Zheng, H. Deng, Z. Yan, Y. Zhao, K. Huang, A. D. Castellano, W. J. Munro, K. Nemoto, D. Zheng, C. P. Sun, Y. X. Liu, X. Zhu, and L. Lu, An efficient and compact switch for quantum circuits, npj Quantum Inf. **4**, 50 (2018).
[31] M. Reagor, C. B. Osborn, N. Tezak, A. Staley, G. Prawiroatmodjo, M. Scheer *et al.*, Demonstration of universal parametric entangling gates on a multi-qubit lattice, Sci. Adv. **4**, eaao3603 (2018).
[32] X. Li, Y. Ma, J. Han, T. Chen, Y. Xu, W. Cai, H. Wang, Y. P. Song, Z.-Y. Xue, Z.-Q. Yin, and L. Sun, Perfect Quantum State Transfer in a Superconducting Qubit Chain with Parametrically Tunable Couplings, Phys. Rev. Applied **10**, 054009 (2018).
[33] T. Fukuhara, P. Schaub, M. Endres, S. Hild, M. Cheneau, I. Bloch, and C. Gross, Microscopic observation of magnon bound states and their dynamics, Nature (London) **502**, 76 (2013).
[34] T. Fukuhara, A. Kantian, M. Endres, M. Cheneau, P. Schaub, S. Hild, D. Bellem, U. Schollwöck, T. Giamarchi, C. Gross, I. Bloch, and S. Kuhr, Quantum dynamics of a mobile spin impurity, Nat. Phys. **9**, 235 (2013).
[35] X. Chen, Z.-C. Gu, Z.-X. Liu, and X.-G. Wen, Symmetry protected topological orders and the group cohomology of their symmetry group, Phys. Rev. B **87**, 155114 (2013).
[36] X. Chen, Z.-C. Gu, Z.-X. Liu, and X.-G. Wen, Symmetry-protected topological orders in interacting bosonic systems, Science **338**, 1604 (2012).
[37] S. de Léséleuc, V. Lienhard, P. Scholl, D. Barredo, S. Weber, N. Lang, H. P. Büchler, T. Lahaye, and A. Browaeys, Experimental realization of a symmetry protected topological phase of interacting bosons with Rydberg atoms, arXiv:1810.13286.
[38] F. Mei, G. Chen, L. Tian, S.-L. Zhu, and S. Jia, Topology-dependent quantum dynamics and entanglement-dependent topological pumping in superconducting qubit chains, Phys. Rev. A **98**, 032323 (2018).
[39] W. P. Su, J. R. Schrieffer, and A. J. Heeger, Solitons in Polyacetylene, Phys. Rev. Lett. **42**, 1698 (1979).
[40] M. Atala, M. Aidelsburger, J. T. Barreiro, D. Abanin, T. Kitagawa, E. Demler, and I. Bloch, Direct measurement of the Zak phase in topological Bloch bands, Nat. Phys. **9**, 795 (2013).
[41] E. J. Meier, F. A. An, and B. Gadway, Observation of the topological soliton state in the Su-Schrieffer-Heeger model, Nat. Commun. **7**, 13986 (2016).
[42] P. St-Jean, V. Goblot, E. Galopin, A. Lemaître, T. Ozawa, L. L. Gratiet, I. Sagnes, J. Bloch, and A. Amo, Lasing in topological edge states of a one-dimensional lattice, Nat. Photonics **11**, 651 (2017).
[43] See Supplemental Material at http://link.aps.org/supplemental/10.1103/PhysRevLett.123.080501 for a discussion of the experimental device and setup, topological magnon insulator states in a qubit chain, the relationship between the single-magnon dynamics and the topological winding number, wave function of zero-energy topological edge states and topological magnon defect states, the influence of qubit lattice size on observing the topological magnon edge states, comparison between experimental data and theoretical expectations in two-dimensional plots, and more simulations with different coupling configurations, which includes Refs. [32–34,38,39,44–50].
[44] R. Barends, J. Kelly, A. Megrant, D. Sank, E. Jeffrey, Y. Chen, Y. Yin, B. Chiaro, J. Mutus, C. Neill, P. O'Malley, P. Roushan, J. Wenner, T. C. White, A. N. Cleland, and J. M. Martinis, Coherent Josephson Qubit Suitable for Scalable Quantum Integrated Circuits, Phys. Rev. Lett. **111**, 080502 (2013).
[45] R. Barends *et al.*, Superconducting quantum circuits at the surface code threshold for fault tolerance, Nature (London) **508**, 500 (2014).
[46] M. Hatridge, R. Vijay, D. H. Slichter, J. Clarke, and I. Siddiqi, Dispersive magnetometry with a quantum limited SQUID parametric amplifier, Phys. Rev. B **83**, 134501 (2011).
[47] T. Roy, S. Kundu, M. Chand, A. M. Vadiraj, A. Ranadive, N. Nehra, M. P. Patankar, J. Aumentado, A. A. Clerk, and R. Vijay, Broadband parametric amplification with impedance engineering: Beyond the gain-bandwidth product, Appl. Phys. Lett. **107**, 262601 (2015).
[48] F. Cardano, A. D'Errico, A. Dauphin, M. Maffei, B. Piccirillo, C. de Lisio, G. D. Filippis, V. Cataudella, E. Santamato, L. Marrucci, M. Lewenstein, and P. Massignan, Detection of Zak phases and topological invariants in a chiral quantum walk of twisted photons, Nat. Commun. **8**, 15516 (2017).
[49] T. Matsubara and H. Matsuda, A lattice model of liquid helium, I, Prog. Theor. Phys. **16**, 569 (1956).
[50] M. Maffei, A. Dauphin, F. Cardano, M. Lewenstein, and P. Massignan, Topological characterization of chiral models

through their long time dynamics, New J. Phys. **20**, 013023 (2018).

[51] X. Gu, A. F. Kockum, A. Miranowicz, Y.-X. Liu, and F. Nori, Microwave photonics with superconducting quantum circuits, Phys. Rep. **718–719**, 1 (2017).

[52] A. C. Potter, T. Morimoto, and A. Vishwanath, Classification of Interacting Topological Floquet Phases in One Dimension, Phys. Rev. X **6**, 041001 (2016).

[53] F. Mei, G. Chen, L. Tian, S.-L. Zhu, and S. Jia, Robust quantum state transfer via topological edge states in superconducting qubit chains, Phys. Rev. A **98**, 012331 (2018).

[54] C. Nayak, S. H. Simon, A. Stern, M. Freedman, and S. Das Sarma, Non-Abelian anyons and topological quantum computation, Rev. Mod. Phys. **80**, 1083 (2008).